PALEOCEANOGRAPHY, VOL. 22, PA4202, doi:10.1029/2006PA001380, 2007

Click Here for Full Article

Lowering of glacial atmospheric CO_2 in response to changes in oceanic circulation and marine biogeochemistry

Victor Brovkin,[1] Andrey Ganopolski,[1] David Archer,[2] and Stefan Rahmstorf[1]

Received 19 October 2006; revised 15 June 2007; accepted 2 July 2007; published 16 October 2007.

[1] We use an Earth system model of intermediate complexity, CLIMBER-2, to investigate what recent improvements in the representation of the physics and biology of the glacial ocean imply for the atmospheric concentration. The coupled atmosphere-ocean model under the glacial boundary conditions is able to reproduce the deep, salty, stagnant water mass inferred from Antarctic deep pore water data and the changing temperature of the entire deep ocean. When carbonate compensation is included in the model, we find a CO_2 drawdown of 43 ppmv associated mainly with the shoaling of the Atlantic thermohaline circulation and an increased fraction of water masses of southern origin in the deep Atlantic. Fertilizing the Atlantic and Indian sectors of the Southern Ocean north of the polar front leads to a further drawdown of 37 ppmv. Other changes to the glacial carbon cycle include a decrease in the amount of carbon stored in the terrestrial biosphere (540 Pg C), which increases atmospheric CO_2 by 15 ppmv, and a change in ocean salinity resulting from a drop in sea level, which elevates CO_2 by another 12 ppmv. A decrease in shallow water $CaCO_3$ deposition draws down CO_2 by 12 ppmv. In total, the model is able to explain more than two thirds (65 ppmv) of the glacial to interglacial CO_2 change, based only on mechanisms that are clearly documented in the proxy data. A good match between simulated and reconstructed distribution of $\delta^{13}C$ changes in the deep Atlantic suggests that the model captures the mechanisms of reorganization of biogeochemistry in the Atlantic Ocean reasonably well. Additional, poorly constrained mechanisms to explain the rest of the observed drawdown include changes in the organic carbon:$CaCO_3$ ratio of sediment rain reaching the seafloor, iron fertilization in the subantarctic Pacific Ocean, and changes in terrestrial weathering.

Citation: Brovkin, V., A. Ganopolski, D. Archer, and S. Rahmstorf (2007), Lowering of glacial atmospheric CO_2 in response to changes in oceanic circulation and marine biogeochemistry, *Paleoceanography*, *22*, PA4202, doi:10.1029/2006PA001380.

1. Introduction

[2] More than 2 decades after their discovery, the cause of the glacial CO_2 cycles remains a scientific challenge [*Broecker and Peng*, 1982; *Archer et al.*, 2000; *Sigman and Boyle*, 2000]. The rise and fall of atmospheric CO_2 concentration is an integral part of the glacial cycles, accounting for about one third of changes in globally averaged temperature over the glacial cycle [*Schneider von Deimling et al.*, 2006b]. In spite of identification of numerous potentially relevant processes, there is still no widespread agreement on mechanisms behind this important internal feedback in the Earth system. Our inability to explain the CO_2 variations of the past undermines our ability to predict the future response of the carbon cycle and climate to anthropogenic carbon emissions [*Scheffer et al.*, 2006; *Torn and Harte*, 2006].

[3] Ice core records show a remarkable correlation between atmospheric CO_2 and Antarctic temperature. This correlation was evident in the original Vostok record to 400 kyr B.P. [*Petit et al.*, 1999] and has recently been extended to 650 kyr B.P. [*Siegenthaler et al.*, 2005]. Paleoclimate records rarely correlate with this degree of reliability and simplicity, spurring a search for a single dominant mechanism, based on or related to the temperature of Antarctica, to explain the glacial CO_2 cycles.

[4] In a number of recent publications it was proposed that a large portion of glacial-interglacial CO_2 variations can be explained by changes in the South Ocean sea ice extent [*Stephens and Keeling*, 2000], Southern Ocean stratification [*Gildor et al.*, 2002], or the Antarctic Bottom Water (AABW) production [*Paillard and Parrenin*, 2004]. The correlation between Antarctic temperature and CO_2 is indeed compelling, but ultimately we need a quantitative mechanism which can explain the atmospheric CO_2 drawdown, a detailed, realistic model that achieves the observed CO_2 drawdown, which has thus far been elusive. The most straightforward mechanism for explaining lower glacial CO_2 is the cooling of the world ocean. CO_2 solubility in seawater increases with decreasing temperature, and the temperature of the deep sea is an obvious place to look. Paleotemperature records of the deep Pacific Ocean based on Mg/Ca ratios of foraminifera show temperature changes of 2°–4°C over glacial cycles [*Martin et al.*, 2002]. Abyssal temperatures have also been reconstructed from pore water $\delta^{18}O$ data by *Adkins et al.* [2002], likewise showing a glacial-interglacial temperature range of 2° to 4°C. A positive feedback between ocean temperature and CO_2

[1]Potsdam Institute for Climate Impact Research, Potsdam, Germany.
[2]Department of Geophysical Sciences, University of Chicago, Chicago, Illinois, USA.

0883-8305/07/2006PA001380$12.00

Table 1. Description of Simulations

Simulation	Factor: Glacial Circulation/SST Changes	Nutrient Utilization in Sub-Antarctic Ocean Atlantic and Indian Sectors	Land Carbon Reduction	Sea Level Change	50% Reduction in Shallow Water Sedimentation[a]
CTRL	no	no	no	no	no
G	yes	no	no	no	no
GN	yes	yes	no	no	no
GNL	yes	yes	yes	no	no
GNLS	yes	yes	yes	yes	no
GNLSC	yes	yes	yes	yes	yes

[a]Imitated by 50% increase in weathering.

would amplify any initial temperature change due to growth of the ice sheets forced by orbital changes [*Archer et al.*, 2004]. This feedback could also ultimately amplify CO_2 concentration changes from fossil fuel combustion [*Scheffer et al.*, 2006; *Torn and Harte*, 2006].

[5] A single core from the Southern Ocean in the *Adkins et al.* [2002] data set revealed an abyssal water mass of extremely high salinity, higher than the increase in ocean mean salinity that resulted from the lowering of sea level. Subsequent reconstruction of the ^{14}C content of deep water from analysis of benthic corals [*Robinson et al.*, 2005], shows that this deep salty water mass was extremely isolated from the atmosphere. Some coupled climate models of the glacial ocean circulation are able to reproduce this stagnant salty water mass by altering the fresh water balance of the Southern Ocean [*Schmittner*, 2003; *Shin et al.*, 2003]. With the colder glacial climate, sea ice is able to survive the trip north to cross the latitude of the polar front. Fresh water carried by the ice leaves behind a polar convection region of higher salinity. This mechanism has been included in recent box model studies [*Köhler et al.*, 2005; *Peacock et al.*, 2006; *Watson and Garabato*, 2006] and a study using an oceanic general circulation model [*Toggweiler et al.*, 2006]. With our model, we are able to simulate explicitly changes in atmospheric and oceanic circulations in response to glacial changes in radiative forcing. Our results in this paper represent the first quantitative assessment of the impact of interactive circulation structure on the atmospheric CO_2, in particular the deep salt stratification in the Southern Ocean [*Adkins et al.*, 2002], including the effects of the sediment $CaCO_3$ feedback to atmospheric CO_2 by the carbonate compensation mechanism via changes in ocean pH [*Broecker and Peng*, 1987; *Archer et al.*, 2000].

[6] Another recent publication by *Kohfeld et al.* [2005] explored evidence for enhanced glacial marine productivity, i.e., the "biological pump," another potential mechanism of lowering glacial CO_2. They found that proxy data support increased marine production during Last Glacial Maximum (LGM) in the Atlantic and Indian sectors of the sub-Antarctic Ocean, north of the Antarctic polar front. South of the front, the proxy data are interpreted as decreased productivity. Data from the Pacific sector of the Southern Ocean are sparse and equivocal. An enhancement of global oceanic marine productivity during the LGM is supported by model studies [e.g., *Bopp et al.*, 2003].

[7] We will show our finding that neither of these mechanisms is sufficient to explain the entire magnitude of the atmospheric CO_2 changes between glacial and interglacial times. The high correlation between CO_2 and temperature spurs a search for a single mechanism, but we are forced to consider the possibility that glacial CO_2 changes are driven not by a single mechanism but a combination of different factors. This strategy is also necessitated by the existence of changes in the carbon cycle in which we are fairly confident, such as changes in shallow water $CaCO_3$ deposition, or the amount of carbon stored in the terrestrial biosphere. In the absence of a single plausible explanation for the CO_2 cycles, we search for a "CO_2 stew" of mechanisms (Table 1) which, combined, can account for the entire CO_2 change, without violation of proxy paleoceanographic constraints on the glacial carbon cycle. This idea is certainly not new [*Archer et al.*, 2000; *Sigman and Boyle*, 2000; *Köhler et al.*, 2005; *Peacock et al.*, 2006], but our challenge is to pursue it with a geographically explicit model, which includes numerous dynamical mechanisms of interactions between climate and biogeochemstry.

2. Methods

[8] Our investigation is based on an Earth system model of intermediate complexity, CLIMBER-2, that is fast enough to carry out simulations on a scale of 10,000 years while its geographical explicitness allows accounting for spatial changes in atmospheric, oceanic, and biogeochemical dynamics. The CLIMBER-2 model includes a 2.5-dimensional statistical-dynamical atmospheric model with $10^\circ \times 51^\circ$ horizontal resolution [*Petoukhov et al.*, 2000], a zonally averaged three-basin dynamic oceanic model based on the work of *Stocker et al.* [1992] with 2.5° meridional resolution and 20 unevenly distributed vertical levels, a one-layer thermodynamic sea ice model with a simple parameterization for horizontal ice transport, a terrestrial biosphere model, an oceanic biogeochemistry model, and a phosphate-limited model for marine biota [*Petoukhov et al.*, 2000; *Ganopolski et al.*, 2001; *Brovkin et al.*, 2002a]. Atmospheric and oceanic components of the version of the CLIMBER-2 model we are using here are essentially the same as in the version used in our early simulation of the LGM climate [*Ganopolski et al.*, 1998; *Petoukhov et al.*, 2000] and the

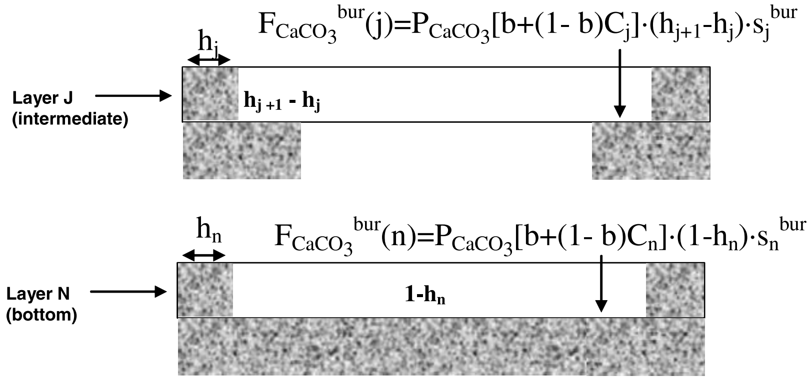

Figure 1. A sketch of carbonate fluxes in the deep ocean. Carbonate flux to the layer *j* is a sum of two fluxes [*Maier-Reimer and Bacastow*, 1990]: a fast sinking fraction *b* of surface $CaCO_3$ production, $b\cdot P_{CaCO3}$, which reaches the ocean floor without dissolution in the water column, and a slow sinking fraction $(1-b) \cdot Cj$, where $Cj = P_{CaCO3} \cdot \exp(\frac{z_{eup}-z}{l})$ exponentially decreases with depth [*Martin et al.*, 1987], *z* is the layer depth (m), z_{eup} = 100 m, *e* folding depth *l* = 3000 m, and *b* = 0.25. Surface $CaCO_3$ flux, P_{CaCO3}, equals $f(T_s)R_rP_{org}$, where P_{org} is export flux at sea surface, R_r is a reference $CaCO_3$:P_{org} ratio (0.12), and $f(T_s)$ is a temperature dependence of the carbonate production (equation (1)). The 10-year moving average of organic and carbonate fluxes accumulated through the year, dust flux (equation (2)), temperature, salinity, total alkalinity, and DIC fields are the input to the carbonate diagenesis model [*Archer et al.*, 2002], which, once a year, calculates a fraction s_j^{bur} of $CaCO_3$ preserved in the sediments. Buried $CaCO_3$ flux, $F_{CaCO3}{}^{bur}(j)$, includes a floor fraction of layer *j*, $h_{j+1} - h_j$ for intermediate layer and $1 - h_j$ for bottom layer, respectively, where h_j is a globally averaged fraction of seafloor at the depth of the layer *j* (hypsometric function).

LGM biogeochemistry [*Brovkin et al.*, 2002b]. However, an important modification has been made in the sea ice components, which explains some differences between results presented here and our early LGM simulations. The early version of CLIMBER-2 includes a purely thermodynamic sea ice model, while the version used here includes a simple parameterization of horizontal sea ice transport. This makes sea ice, especially under the glacial climate conditions, an important contributor to the surface freshwater flux and explained a much large change in the ocean salinity as compared to that reported by *Ganopolski et al.* [1998]. Mobility of sea ice is a crucial part of many theories of the glacial carbon cycle [*Keeling and Stephens*, 2001; *Shin et al.*, 2003].

[9] Carbonate compensation is simulated by a model of deep sea sediment diagenesis [*Archer*, 1991] coupled to CLIMBER-2 (see Figure 1). The sediment model operates on the CLIMBER-2 spatial resolution with one extension: While the ocean model has vertical basin boundaries, the sediment model accounts for realistic oceanic hypsometry by calculating the fractional area of the grid cell floor at every intermediate model depth (14 layers from 500 to 5000 m). Surface carbonate production ceases with sea surface temperatures (SSTs) lower than 10°C [see, e.g., *Iglesias-Rodríguez et al.*, 2002]. This is captured in the model by a reduction in $CaCO_3$ production by a factor *f* which is a semiempirical function of SST, T_s:

$$f(T_s) = \frac{e^{T_s - T_0}}{5 + e^{T_s - T_0}}, \qquad (1)$$

where T_0 is equal to 3.5°C [*Maier-Reimer and Bacastow*, 1990].

[10] The flux of dust to the seafloor, r_{clay}, is estimated by a correlation with organic production, r_{org}, based on the present-day detrital rain rate to the seafloor [*Archer et al.*, 2002]:

$$r_{clay} = 1.8 \cdot 10^{-15} \cdot (r_{org})^{1.41}. \qquad (2)$$

The production ratio of $CaCO_3$ to organic carbon in the surface ocean is a product of a reference "rain ratio," R_r, and a temperature-dependent factor $f(T_s)$ (equation (1)). A value of the R_r parameter, 0.12, is tuned to best reproduce observed fields of dissolved inorganic carbon (DIC) and alkalinity (ALK) in the preindustrial simulation CTRL. In general, the coupled model tends to overestimate near-surface concentration of phosphate in the tropical regions, but in the intermediate to deep ocean, distributions of phosphate, DIC and ALK are in good agreement with the data (for details, see *Brovkin et al.* [2002a]). Simulated global $CaCO_3$ export flux, 0.85 Pg C/yr (Table 2), was within a wide range of $CaCO_3$ export estimates from 0.5 to 2.0 Pg C/yr [*Iglesias-Rodríguez et al.*, 2002; *Feely et al.*, 2004; *Jin et al.*, 2006]. It is also within a more narrow range of estimates based on alkalinity observations (0.6–1.4 Pg C/yr [*Jin et al.*, 2006]). The global mean value of the $CaCO_3$ to organic carbon ratio was 0.11 (0.85:7.7, see Table 2). This value is slightly higher than a value of 0.1 used in the reference CLIMBER-2 version without sedimentation [*Brovkin et al.*, 2002a], but it is close to a range of 0.07 to 0.1 found in the model experiments by *Jin et al.* [2006].

Table 2. Model Results

Simulation	Atmospheric CO_2 After Carbonate Compensation, ppmv	Atmospheric CO_2 Without Carbonate Compensation,[a] ppmv	Organic Export Flux at 100 m Depth, Pg C/yr	Export $CaCO_3$ Flux at 100 m Depth, Pg C/yr	ALK_{ave}, μmol/kg	DIC_{ave}, μmol/kg	Atmospheric $\delta^{13}CO_2$, ‰
CTRL	280	-	7.7	0.85	2373	2233	−6.50
G (circulation and SST)	237	246	7.4	0.81	2410	2262	−6.48
GN (G plus nutrients)	200	211	9.2	0.85	2437	2284	−6.20
GNL (GN plus land)	215	243	9.2	0.85	2502	2352	−6.61
GNLS (GNL plus sea level)	227	251	9.3	0.86	2573	2423	−6.60
GNLSC (GNLS plus coral reefs)	215	-	9.3	0.86	2630	2459	−6.64

[a]In the CTRL simulation, weathering equals sedimentation; therefore atmospheric CO_2 is 280 ppmv with or without compensation. The GNLSC simulation without compensation was not performed because changes in shallow water sedimentation affect atmospheric CO_2 through the carbonate compensation mechanism.

[11] Shallow water carbonate sedimentation, organic carbon weathering and burial were neglected in the CTRL simulation. Surface alkalinity and DIC fields were permanently updated to compensate for the carbonate buried in the deep sea. In the equilibrium simulation integrated for 50,000 years, deep sea carbonate burial was 0.11 Pg C/yr (9.4 Tmol/yr). This value is slightly higher than 8.3 Tmol/yr of present-day $CaCO_3$ burial in deep sea estimated by *Catubig et al.* [1998] but well within a range of 0.1 to 0.14 Pg C/yr suggested recently by *Feely et al.* [2004]. It is also very close to a value of 10 Tmol/yr obtained in the experiments with carbonate sediment model by *Ridgwell and Hargreaves* [2007]. Because shallow water sedimentation was ignored in our simulations, we prescribed a part of the weathering which balances the deep sea burial, or deep-sea influx [*Archer and Maier-Reimer*, 1994] to the deep sea burial of $CaCO_3$ predicted by the sediment model (9.4 Tmol/yr). Prescribing weathering flux to the burial flux is opposite to what found in reality [*Broecker and Peng*, 1987; *Ridgwell and Zeebe*, 2005], but this method guarantees that the model is staying at equilibrium with alkalinity and DIC inventories close to observations. This approach is often used in sediment modeling studies which do not account for the shallow water carbonate sedimentation [e.g., *Ridgwell and Hargreaves*, 2007].

[12] A list of simulations is shown in Table 1. We performed five glacial simulations with five factors added consecutively, one factor after another. We started from a glacial climate simulation (G), then added enhanced nutrient utilization in the subpolar Southern Ocean (GN), land carbon release (GNL), sea level change (GNLS), and reduction in shallow water carbonate sedimentation (GNLSC). Details of these simulations are explained in section 3.

[13] In all glacial simulations G to GNLSC, the radiative effect of the CO_2 concentration was imposed (constant) in order to exclude the complicating effect of the climate to CO_2 feedback. Since a radiative scheme of CLIMBER-2 accounts only for one well mixed greenhouse gas, CO_2, the impacts of low LGM CH_4 and N_2O concentrations are accounted for by using in the radiative scheme the so-called "equivalent" CO_2 concentration instead of the actual CO_2 concentration. Assuming LGM CO_2 concentration of 200 ppmv and the combined radiative forcing of glacial-interglacial changes in CH_4 and N_2O of -0.7 W/m^2, the "equivalent" LGM CO_2 concentration was set to 180 ppmv. The radiative effect of the elevated dust concentration in the glacial atmosphere was not accounted for (according to simulations by *Schneider von Deimling et al.* [2006b], this forcing could lead to an additional 1°C global cooling). The distribution of ice sheets and changes in elevation and land area were prescribed following *Peltier* [1994], and orbital forcing was taken as of 21,000 years B.P. [*Berger*, 1978]. The ice sheets were assumed to be in equilibrium, hence amount of freshwater corresponding to accumulated snow over the ice sheets was released in the nearest oceanic grid cell. The same river routing scheme was used for control and glacial simulations.

[14] Silicate weathering, volcanic CO_2 outgassing, shallow water carbonate sedimentation, as well as organic carbon weathering and burial were neglected. The sedimentary feedback to ocean pH, calcium carbonate compensation, was active in all glacial simulations. For comparison with the other studies, we also performed simulations G, GN, GNL, and GNLS without carbonate compensation and reported equilibrium CO_2 concentrations after 10,000 years in the Table 2. Dust deposition input to the sediment model for glacial time was doubled from the control simulation to account for increased dust load during the LGM [*Rea*, 1994; *Mahowald et al.*, 1999]. Simulations with carbonate compensation were integrated for 50,000 years to allow the weathering and sedimentary $CaCO_3$ cycle to approach equilibrium. Each simulation took about 100 hours of single processor time on the IBM p655 cluster.

3. Results

3.1. Simulated Glacial Climate

[15] The climate model under a complete set of glacial forcings (except dust, see above) simulates a global surface air temperature cooling by 5°C, and globally averaged SST and volume averaged ocean temperature decreased by 3°C. The main changes in oceanic circulation are associated with a weakening (by ~20%) and a considerable shoaling of the Atlantic meridional overturning cell and intensification of Antarctic bottom water (AABW) formation, with a much stronger penetration of AABW into the Atlantic Ocean. While in the present-day CTRL simulation AABW is present only in the southern Atlantic (Figure 2a), in the

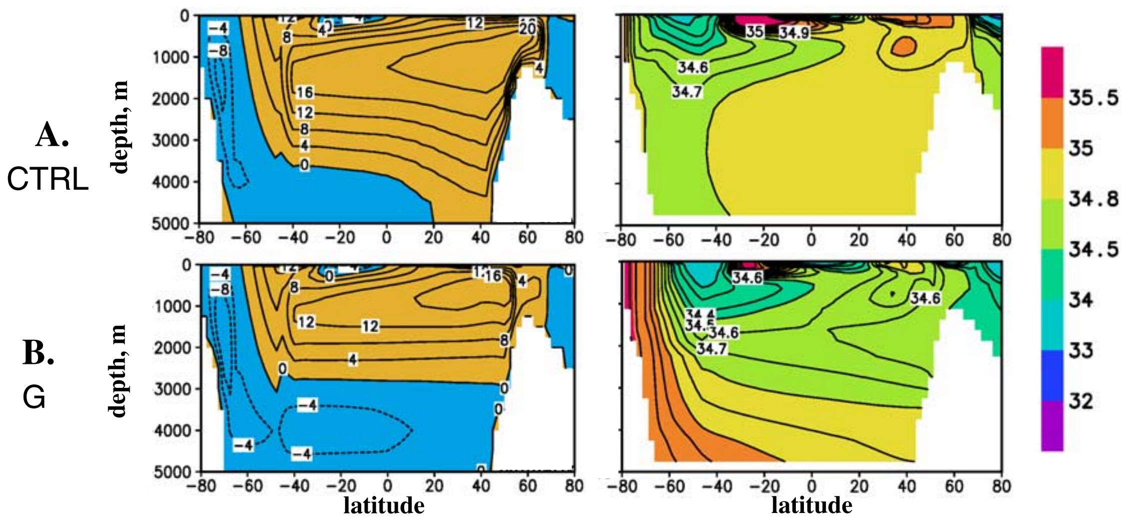

Figure 2. Simulated circulation and salinity in the Atlantic basin for (a) present-day simulation CTRL and (b) glacial simulation G. (left) Overturning (Sv), orange and blue colors are for clockwise and counterclockwise circulations, respectively, and (right) salinity (psu) are shown.

glacial simulations AABW fills the whole Atlantic basin below 2500 m (Figure 2b).

[16] Enhanced formation and increased density of AABW water masses is primarily caused by more extensive sea ice formation with associated brine rejection around Antarctica. The simulated maximum Southern Hemisphere sea ice area under LGM condition is twice as large as at present (Figure 3) which agrees well with recent glacial sea ice reconstruction [*Gersonde et al.*, 2005]. In particular, in the Atlantic sector of the Southern Ocean the wintertime sea ice edge at LGM is located around 45°S, about 1000 km northward of its present-day position, consistent with the paleoceanographic data. This large sea ice expansion leads to an increase of the sea ice transport out of the area of AABW formation, which increases the salinity of AABW by 0.5 psu (in addition to the 1 psu of global increase of salinity due to sea level drop) and decreases surface salinity in the Atlantic Ocean (Figure 2b). The simulated increase of AABW salinity is consistent although somewhat smaller than the deep pore water estimates by *Adkins et al.* [2002]. Although North Atlantic deep water (NADW) cools more than AABW under the glacial conditions, the relative increase of AABW salinity and a relative decrease of NADW salinity overwhelms the temperature effect and the density of glacial AABW becomes higher than the density of NADW. This allows AABW to occupy a much larger portion of the deep Atlantic, and causes a shoaling and a weakening of the Atlantic meridional circulation. In the Pacific, there is little change in the circulation field, but changes in temperature are comparable to the Atlantic and similar to reconstructions by *Martin et al.* [2002] (Figure 4a).

3.2. Modeled Glacial Biogeochemistry

3.2.1. Simulation G: Effect of Changes in Circulation and Sea Surface Temperatures

[17] Temporal dynamics of atmospheric CO_2 in the G simulation (Figure 5) demonstrates several stages of the model response to the imposed glacial boundary conditions. During the first 500 years, CO_2 drops by 18 ppmv in response to the surface ocean cooling. The CO_2 drawdown by additional 15 ppmv during the next 2000 years is a response to the reorganization of the oceanic circulation. Acidification of deep waters leads to a temporary reduction in carbonate sediment preservation until a balance between weathering and sedimentation is achieved. This process results in increased total oceanic alkalinity which decreases atmospheric CO_2 further. A further slow decrease by about 10 ppmv is associated with carbonate compensation. The full drawdown of atmospheric CO_2 after carbonate compensation is 43 ppmv (Table 2). The average temperature

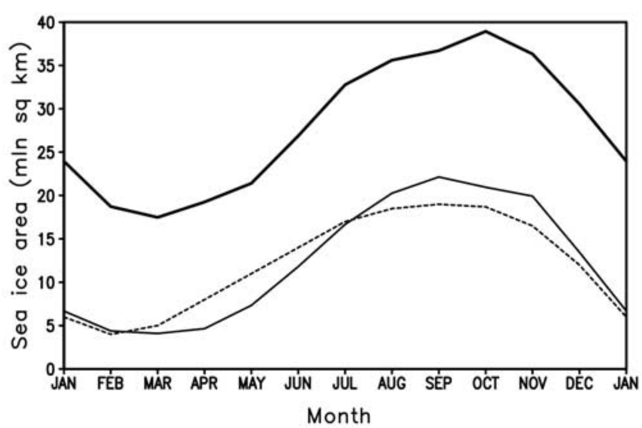

Figure 3. Seasonal variations of sea ice area (10^6 km^2) in the Southern Hemisphere. Thin solid line shows simulated modern climate, thick solid line shows simulated LGM climate, dashed line shows present-day observations based on the Hadley Centre Sea Ice and Sea Surface Temperature data set [*Rayner et al.*, 2003].

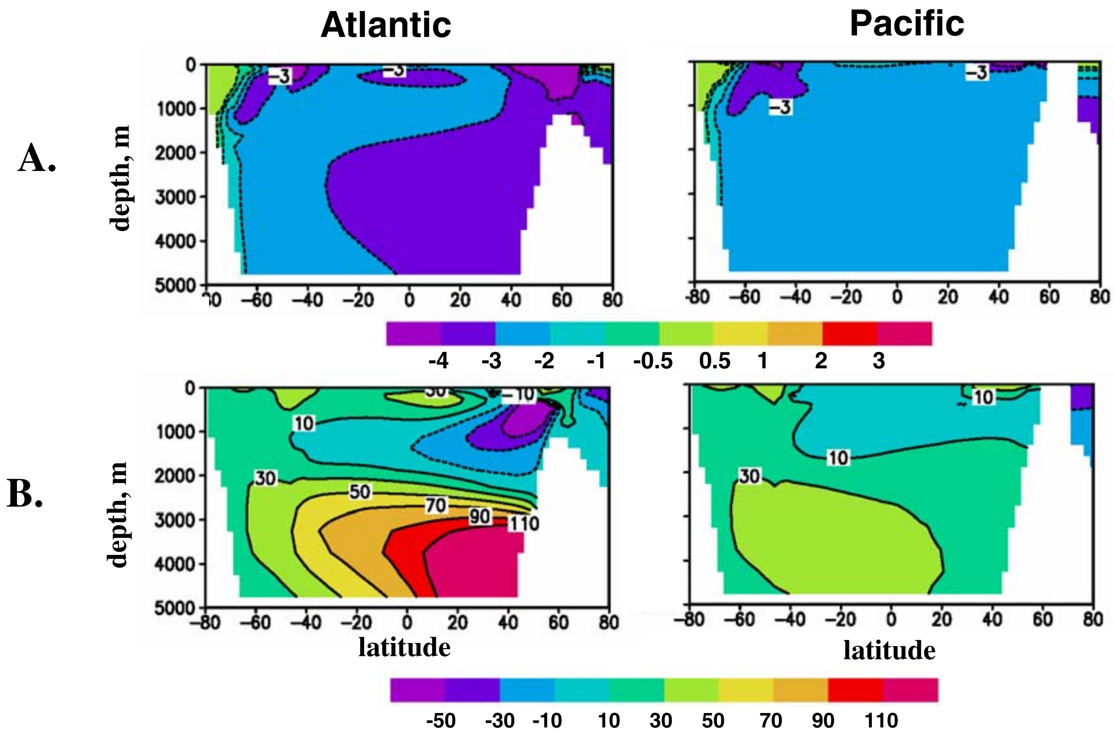

Figure 4. Glacial oceanic changes: (a) temperature (°C) and (b) DIC distribution (μmol/kg). Shown is a difference in these tracers between simulations G and CTRL.

decrease of the ocean was 3°C, therefore the equilibrium sensitivity of atmospheric CO_2 to the oceanic temperature change amounts to 14 ppmv/°C. This is higher than the 6–10 ppmv/°C estimate from a set of solubility experiments using several oceanic general circulation models (GCM) [*Martin et al.*, 2005], in part because of the increase in volume of the high-carbon AABW water mass which was not accounted for in those models. The maximum increase in the DIC concentration, 100 μmol/kg, is found in the deep North Atlantic, where the boundary between AABW and NADW has changed (Figure 4b). Without circulation changes and carbonate compensation, simulated atmospheric CO_2 sensitivity to the SST change would be only 18 ppmv per 3°C or 6 ppmv/°C as seen on Figure 5, in line with results by *Martin et al.* [2005].

3.2.2. Simulation GN: G Plus Iron Fertilization

[18] In the GN simulation, the biological pump in the Atlantic and Indian sectors of the sub-Antarctic Ocean (30° to 50°S) was stimulated to complete drawdown of nutrient (PO_4) in the surface ocean imitating a productivity increase during LGM in these regions detected by *Kohfeld et al.* [2005], probably the result of iron fertilization from Patagonian dust [*Mahowald et al.*, 1999]. Since the model does not include an iron cycle, the phytoplankton productivity in these regions was calculated assuming complete utilization of PO_4 at the surface. The globally averaged export flux at the surface increased by 1.8 Pg C/yr (24%)

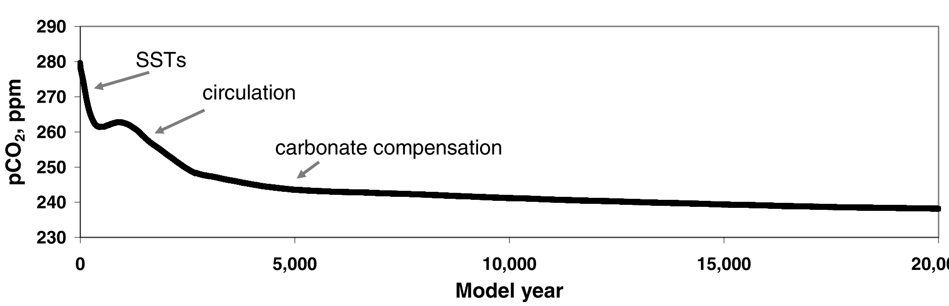

Figure 5. Dynamics of atmospheric CO_2 (ppmv) in the G simulation. Initial conditions were from the CTRL simulation. Imposed glacial boundary conditions are explained in text. Arrows indicate time periods of dominant mechanisms.

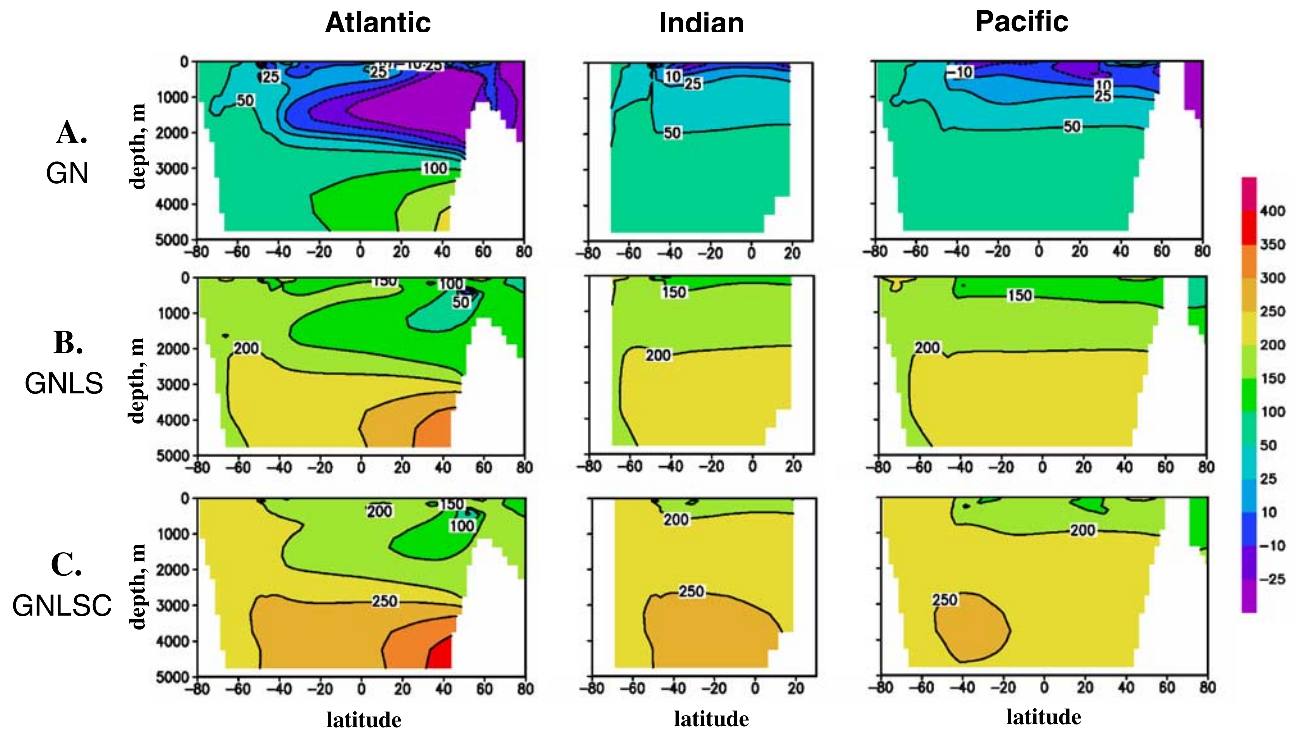

Figure 6. Glacial changes in oceanic DIC distribution (μmol/kg): (a) simulation GN, (b) simulation GNLS, and (c) simulation GNLSC. Shown is a difference in these tracers between the given simulation and simulation CTRL.

and atmospheric CO_2 dropped by 37 ppmv in comparison with the G simulation (Table 2). This value is higher than the 15-ppmv effect found by *Bopp et al.* [2003] in an ocean-biogeochemistry model run driven by the LGM boundary conditions and dust flux, but that simulation had only 6% increase in global export production. *Bopp et al.* [2003] did not include the effect of carbonate compensation, but this effect is very small in the GN simulation: Without compensation, the atmospheric CO_2 difference between the GN and the G simulations is 35 ppmv (Table 2), or only 2 ppmv less than with the compensation. If $CaCO_3$ production were increased proportionally with organic carbon production, the resulting increase in $CaCO_3$ burial would act to acidify the ocean as weathering/burial steady state is restored, increasing pCO_2 by the $CaCO_3$ compensation mechanism [*Archer et al.*, 2000]. However, because an increase in productivity was limited to subantarctic regions with low SSTs, an increase in $CaCO_3$ export flux was less pronounced than an increase in organic carbon export and globally averaged rain ratio decreased to 0.09 (0.85:9.2, Table 2).

[19] In comparison with the G simulation (Figure 4b), the DIC concentration mainly increased in Southern Ocean and deep ocean (Figure 6a). This increase is pronounced not only in the Atlantic and Indian oceans where the forcing was applied, but also in the Pacific Ocean, which is linked to the Atlantic and Indian through the Southern Ocean.

3.2.3. Simulations GNL and GNLS: GN Plus Land Carbon Plus Sea Level Change

[20] While the GN simulation explains almost the complete magnitude of glacial CO_2 changes, we should not neglect several other factors that worked in the opposite direction. Terrestrial pollen records reveal that during the LGM, forest cover was strongly reduced: Boreal forests were diminished because of ice sheet expansion and increased aridity of continental interiors, while tropical forests had a more open canopy due to increased aridity [*Crowley*, 1995; *Prentice and Jolly*, 2000]. Reduced atmospheric CO_2 levels should have a direct negative effect on the plant productivity through reduced water use efficiency [*Harrison and Prentice*, 2003]. Much of the land surface in the high northern latitudes was covered by ice sheets, although this reduction in forested area was partly compensated for by exposed tropical shelf areas in Southeast Asia, likely populated by forest [e.g., *Otto et al.*, 2002].

[21] The glacial reduction in forest cover simulated by the CLIMBER-2 model leads to a cooling of about 1°C because of increased surface albedo and reduced transpiration [*Jahn et al.*, 2005]. These biogeophysical effects are accounted for in the glacial simulations reported here. Several model studies that account for climate, CO_2, and sea level changes during the LGM suggest a net reduction of terrestrial carbon storage by 440–720 Pg C [*Francois et al.*, 1999], 820 to 850 Pg C [*Joos et al.*, 2004], and 820 to 1100 Pg C [*Otto et al.*, 2002]. Low glacial CO_2 concentration is the main factor affecting carbon storage in these simulations. Pollen-based reconstruction by *Crowley* [1995] suggests glacial decrease in land carbon in the range of 760 to 1040 Pg C. Independently, glacial changes in deep ocean $\delta^{13}C$ have been interpreted as a reduction in land carbon storage by about 300–700 Pg C [*Shackleton*, 1977; *Duplessy et al.*, 1988;

Bird et al., 1994], although glacial-interglacial changes in the deep sea $\delta^{13}C$ could be also interpreted as changes in global storage of methane hydrates [*Maslin and Thomas*, 2003]. The interactive terrestrial biosphere model in CLIMBER-2 predicts a net reduction in terrestrial carbon storage by 540 Pg C using prescribed glacial CO_2 of 185 ppmv, glacial changes in sea-land mask, and climate from the G simulation [*Jahn et al.*, 2005]. Biomass and soil storages are lower by 190 Pg C and 350 Pg C, respectively, and about 50% of the total carbon decline is due to lowering of CO_2. Accounting for the land carbon release in the GNL simulation results in an atmospheric CO_2 increase by 15 ppmv after carbonate compensation (Table 2). This value is in line with estimates of 15 ppmv by *Sigman and Boyle* [2000] and 17 ppmv by *Archer et al.* [2000] for 500 Pg C land carbon release. Without carbonate compensation, the predicted effect of the land carbon on CO_2 is twice as large (32 ppmv, see Table 2).

[22] The buildup of ice sheets during glacial time led to reduced sea level that reached its lowest point during the LGM. In the GNLS simulation, we assumed that a 3% decrease in total ocean volume was accompanied by a 3% increase in salinity, alkalinity, and PO_4 concentrations. The initial DIC concentration was unchanged and total oceanic DIC inventory was reduced by 3%. The excessive CO_2 was initially allocated to the atmosphere in order to conserve carbon in the land-atmosphere-ocean system. In equilibrium response to these changes, atmospheric CO_2 increased by 12 ppmv after compensation, very similar to the 14 ppmv increase suggested by *Broecker and Peng* [1987]. Before compensation, the CO_2 increase was less (8 ppmv, Table 2). The effect of carbonate compensation on atmospheric CO_2 might be explained by a slight but globally uniform increase in carbonate production in this simulation (Table 2), see discussion of effect of iron fertilization by *Archer et al.* [2000].

[23] Together, these land carbon and sea level effects lead to an increase in atmospheric CO_2 by 27 ppmv after carbonate compensation. The oceanic DIC concentration is considerably increased (by about 150 μmol/kg) in comparison with the GN simulation (Figure 6b). This is mostly a sign of dissolved land carbon amplified by the carbonate compensation process, with a further contribution from the drop in sea level (Table 2).

3.2.4. Simulation GNLSC: GNLS Plus Reduction in Shallow Water Sedimentation

[24] During the glacial period, coral reef area in tropical and subtropical shelf regions was greatly reduced. Simulations of the ReefHab model by *Kleypas* [1997] suggested an almost fourfold reduction in coral reef production during the LGM. Our more mild assumption here is that carbonate sedimentation in shallow waters was reduced by 50% during the glacial time. We assume that shallow water sedimentation is approximately equal to deep-sea carbonate sedimentation at present [*Milliman and Droxler*, 1996], although a recent review by *Feely et al.* [2004] suggests relatively higher accumulation of $CaCO_3$ in continental shelf sediments (0.13 to 0.17 Pg C/yr) than along the continental margins or in the deep sea (0.1 to 0.14 Pg C/yr).

[25] Our model does not include shallow water sedimentation. In the real ocean, a decrease in shallow water $CaCO_3$ burial driven by a change in shelf area would manifest itself as an increasing weathering load which deep sea $CaCO_3$ burial must accommodate. Assuming that shallow water $CaCO_3$ burial is unresponsive to changes in ocean chemistry, we can impose the impact of changes in shelf area by changing the net weathering rate to the deep sea. An increase in terrestrial weathering flux ultimately leads to increase in the deep sea burial. Carbonate burial in the deep sea in equilibrium present-day simulation CTRL is compensated by a terrestrial weathering flux of the same value (0.11 Pg C/yr). A 50% decrease in shallow water sedimentation manifested itself as a net weathering flux 50% higher in the GNLSC simulation. This results in further enhancement of the DIC and alkalinity concentrations and a consequent atmospheric CO_2 drop by 12 ppmv (Figure 6c and Table 2). In the steady state, ocean carbonate ion increase makes the deep ocean more basic, until deep ocean $CaCO_3$ burial balances the weathering flux. Ultimately, this scenario leads to an increase in deep sea carbonate ion concentration and a deepening of the lysocline or carbonate compensation depth (CCD).

[26] Figure 7 presents a comparison of the fraction of $CaCO_3$ (wt %) in the upper sediment layer. While a comparison of present-day observations averaged to the CLIMBER-2 grid (Figure 7a) with model results in the CTRL simulation (Figure 7b) shows clearly that the model performance is far from perfect, it is able to capture several important features of the carbonate distribution on the ocean floor. First, the present-day CCD is located deeper in the North Atlantic than in the South Atlantic, and this is reproduced by the model. Secondly, the difference between Atlantic and Pacific basins is captured quite well, as the CCD in the Pacific is shallower than in the Atlantic. These CCD differences are explained by less corrosive deep waters in North Atlantic relatively to the South Atlantic and Pacific [see *Archer*, 1996; *Ridgwell and Zeebe*, 2005]. The strong $CaCO_3$ burial in the North Pacific is due to overestimation of the biological production there (see discussion of *Brovkin et al.* [2002a]).

[27] The CCD depth is not substantially changed in the simulation GNLS (Figure 7c) relatively to the CTRL simulation (Figure 7b). This is expected because carbonate compensation restores the deep-sea carbonate ion concentration to something close to the CTRL value. In the GNLSC simulation the CCD deepens by about 500 m, resulting in a sedimentation shift to the model ocean floor of 5000 m in the Southern Ocean (Figure 7d). This is, perhaps, a stronger shift than would be supported by the glacial CCD reconstruction [*Catubig et al.*, 1998; *Anderson and Archer*, 2002].

3.2.5. Other Mechanisms: Changes in Rain Ratio, Weathering, Nutrients Utilization in Pacific

[28] Another mechanism that may have contributed to the lower glacial atmospheric CO_2 is a decrease in carbonate to organic flux ratio [*Archer and Maier-Reimer*, 1994]. This mechanism involves a shift from calcite- to silicate-producing plankton during glacial periods, for example via the silica leakage mechanism [*Matsumoto et al.*, 2002].

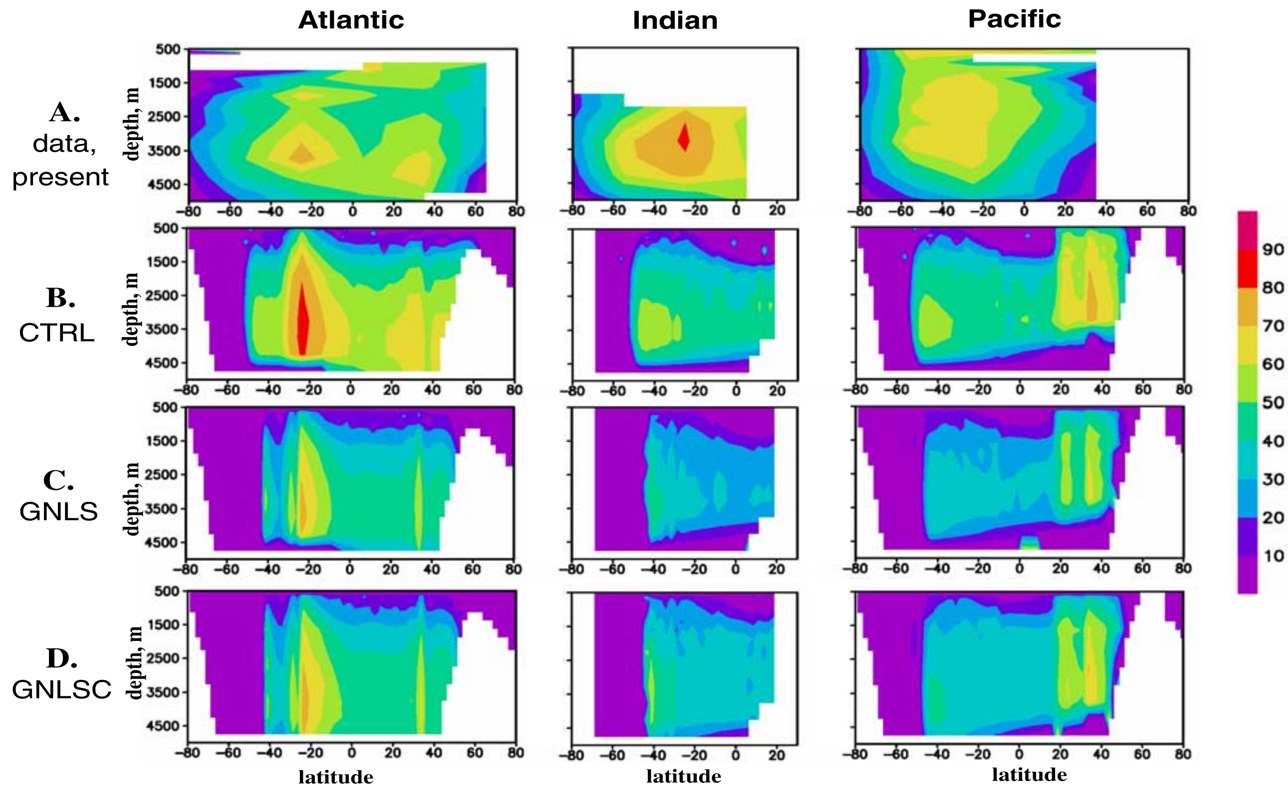

Figure 7. CaCO3 (wt %) in top layer of sediments. (a) Observations [*Archer*, 1996] averaged on the CLIMBER-2 grid with three-basin and 10° latitudinal resolution. The sedimentary data were binned according to water depth and latitude and averaged, weighted according to seafloor area. Shallower bins had only slope settings and occasional seamounts. (b) Simulation CTRL. (c) Simulation GNLS. (d) Simulation GNLSC.

CLIMBER-2 does not simulate phytoplankton structure, but we tested the mechanism by reducing the rain ratio from 0.12 to 0.1 in simulation GN. The ocean carbonate burial rate initially decreases, driving the ocean toward the basic. The change in the equilibrium ocean chemistry reduces CO_2 by an additional 15 ppmv (Table 3).

[29] During the glacial maximum, river runoff was different from the Holocene because of the large area covered

Table 3. Mechanism Contributions to Glacial Atmospheric CO_2 Changes

Mechanism	Simulated ΔCO_2 After Carbonate Compensation, ppmv	Proxy Data in Support of the Model Results
	Mechanisms Well Supported by Proxy Data	
Circulation and SST	−43	oceanic $\delta^{13}C$ [*Duplessy et al.*, 1988; *Curry and Oppo*, 2005]
Sea level	12	oceanic $\delta^{18}O$, corals [*Lambeck and Chappell*, 2001; *Waelbroeck et al.*, 2002]
Nutrient utilization in sub-Antactic, Atlantic and Indian oceans	−37	Cd/P, ^{15}N, $\delta^{13}Si$, [*Elderfield and Rickaby*, 2000; *Kohfeld et al.*, 2005]
Land carbon	15	pollen records and oceanic $\delta^{13}C$ [*Bird et al.*, 1994; *Crowley*, 1995; *Joos et al.*, 2004]
Shallow water carbonate sedimentation	−12	carbonate sediments and corals [*Milliman*, 1993; *Milliman and Droxler*, 1996]
Subtotal	−65	
	Less Certain Mechanisms	
10% decrease in weathering	2	
20% decrease in rain ratio	−15	
Nutrients utilization in subantarctic Pacific Ocean	−7	
Total	−85	

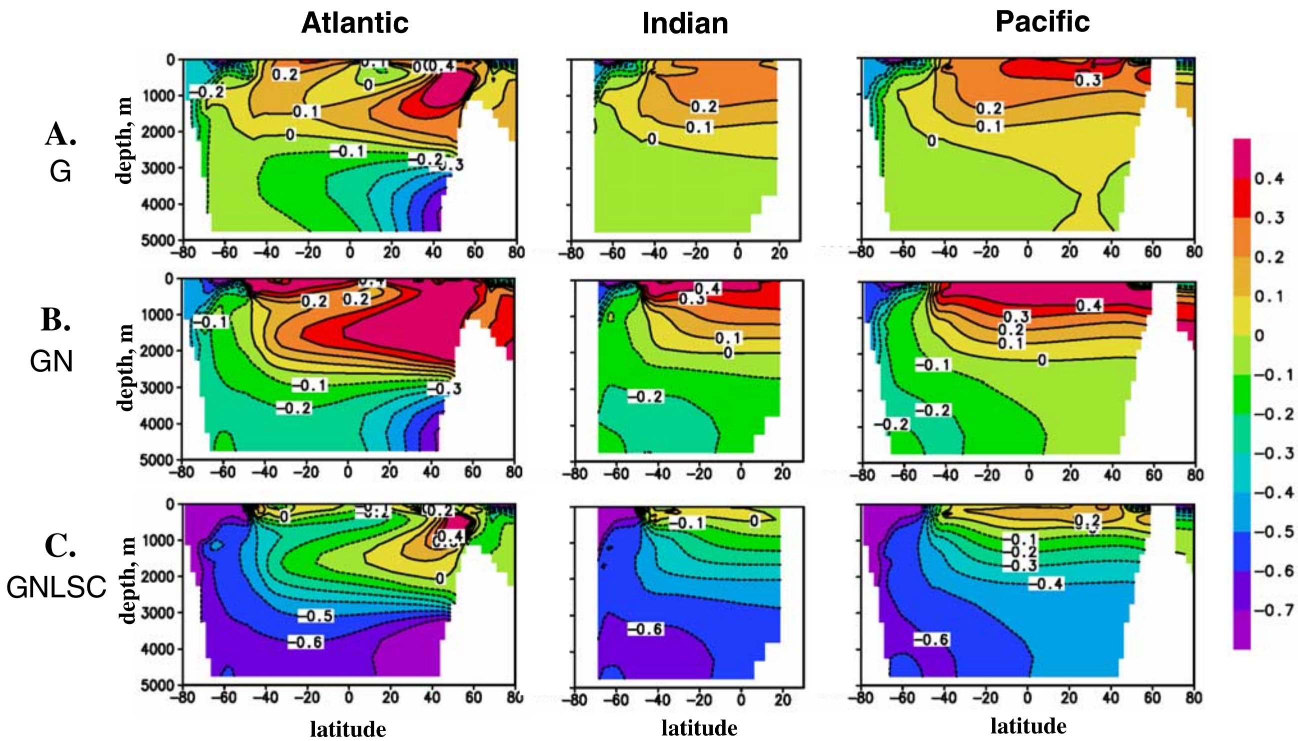

Figure 8. Glacial changes in oceanic δ^{13}C distribution (‰): (a) simulation G, (b) simulation GN, and (c) simulation GNLSC. Shown is a δ^{13}C difference between the given simulation and simulation CTRL.

with ice sheets, exposed shelf areas, and drier climate. Glacial changes in terrestrial weathering (even direction of these changes) are uncertain, but they were unlikely to be high [*Munhoven*, 2002; *Foster and Vance*, 2006]. As a pure sensitivity test, we investigated a scenario of a 10% reduction in the terrestrial weathering flux and found an atmospheric CO_2 increase by 2 ppmv in response (Table 3).

[30] *Kohfeld et al.* [2005] did not detect large glacial changes in productivity in the Pacific sub-Antarctic Ocean, but this region is poorly populated with data. We performed an additional model simulation with complete nutrient utilization in this region. The CO_2 drawdown is 7 ppmv, much less than 37 ppmv in case of the Atlantic and Indian sub-Antarctic Ocean (Table 3). This could be explained by the very small changes in glacial Pacific circulation as compared to the glacial circulation changes in the Atlantic. Additionally, surface nutrient concentrations in the Pacific sub-Antarctic Ocean were already drawn down by complete utilization of surface nutrients in the Atlantic and Indian sectors of the sub-Antarctic Ocean.

3.2.6. Redistribution of δ^{13}C

[31] The distribution of δ^{13}C in the ocean is driven by several factors simultaneously: changes in ocean circulation, biological pump, and land carbon storage. In the Atlantic, a change in the water mass distribution in the G simulation results in a decrease in δ^{13}C below 2000 m, with a maximum decrease in the deep North Atlantic, while δ^{13}C in the upper ocean increases (Figure 8a). The subantarctic biological pump enhancement in the GN simulation leads to a further increase in the δ^{13}C gradient between upper and deeper waters (Figure 8b), and a stronger decrease in δ^{13}C in the Antarctic Ocean. These changes are qualitatively in line with reconstructions of δ^{13}C distribution in the Atlantic by *Duplessy et al.* [1988] and more recent synthesis of glacial δ^{13}C changes in West Atlantic [*Curry and Oppo*, 2005]. Release of terrestrial carbon in the GNL, GNLS, and GNLSC simulations causes an average δ^{13}C change in the ocean of −0.4‰ (Figure 8c), a bit more than the usual estimate of −0.35‰ [*Shackleton*, 1977].

[32] When compared with the reconstruction of glacial-interglacial δ^{13}C changes by *Duplessy et al.* [1988], decrease in δ^{13}C in the deep North Atlantic is reproduced quite well by the model (Figure 9) although a shoaling of NADW in our simulation is not as substantial as in the reconstruction. The same is true for the deep Southern Ocean, although the data suggest where much stronger decrease in δ^{13}C. In the Indian and Pacific basins, δ^{13}C increases above 2000 m depth (not shown).

[33] Ice core measurements of atmospheric $\delta^{13}CO_2$ during the LGM [*Smith et al.*, 1999] reveal little change between LGM and Holocene. The average LGM value of $\delta^{13}CO_2$ is about −6.6‰, which is only by 0.1‰ smaller than the Holocene value (−6.5‰). If $\delta^{13}CO_2$ were influenced by changes in land carbon only, changes in $\delta^{13}CO_2$ should be about 0.3–0.4‰. This suggests that atmospheric $\delta^{13}CO_2$ is controlled not only by the land carbon balance but also other factors such as changes in oceanic circulation and marine biology [*Brovkin et al.*, 2002b]. In the G simulation with circulation changes only, atmospheric $\delta^{13}CO_2$ was not affected at all (Table 3), despite a decrease in δ^{13}C in the

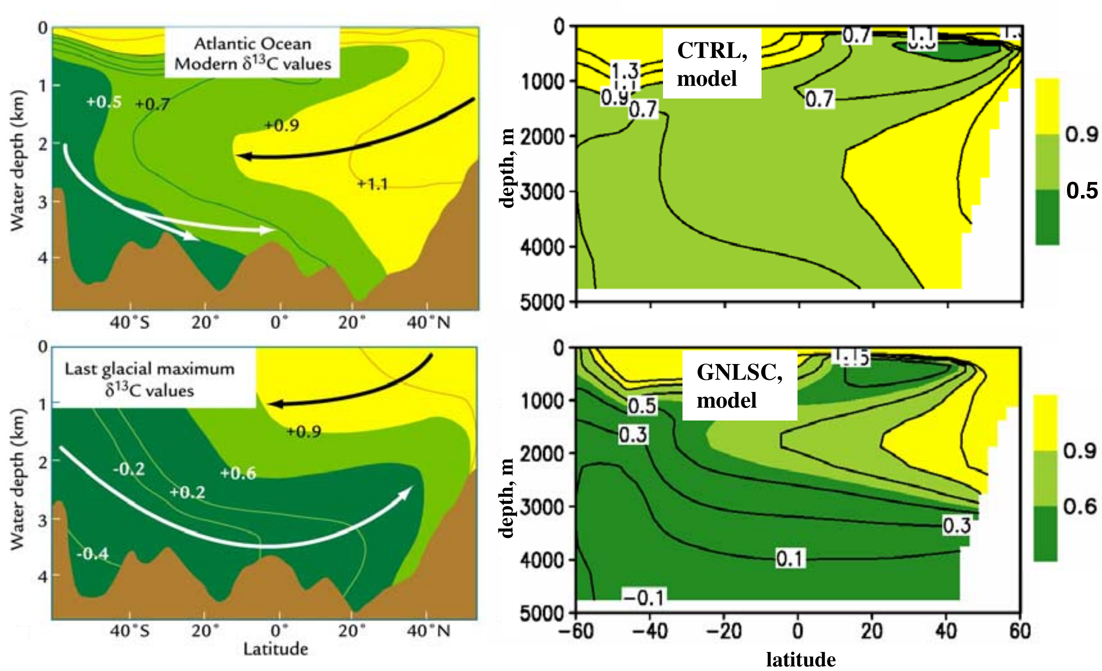

Figure 9. (left, top) Modern and (left, bottom) glacial distribution of δ^{13}C in Atlantic (‰). Figure 9 left is from *Duplessy et al.* [1988] modified version reproduced from *Ruddiman* [2001]. © 2001 by W. H. Freeman and Company. (right) Results from the (top) CTRL and (bottom) GNLSC simulations. The color bar to the right is for the model results. Isolines interval is 0.2‰.

deep Atlantic. This is caused by a redistribution of ocean ^{13}C, with an increase in the surface Atlantic and Pacific (Figure 8a). In the GN simulation, an enhanced biological pump amplified the δ^{13}C gradient between deep and surface waters and led to an increase of atmospheric $\delta^{13}CO_2$ by 0.3‰. Land carbon release in the GNL simulation draws $\delta^{13}CO_2$ down by 0.4‰ to a level of −6.6‰, in line with ice core data. Other factors, such as sea level change, did not significantly contribute.

4. Discussion

[34] Coupled model simulations of the glacial climate published to date show no consistency in changes of the Atlantic ocean circulation. Some models show a pronounced weakening and shoaling of the Atlantic meridional overturning circulation [e.g., *Kim et al.*, 2003; *Shin et al.*, 2003], and others show the opposite [e.g., *Hewitt et al.*, 2001; *Kitoh et al.*, 2001]. The latest set of LGM experiments performed with several GCMs and models of intermediate complexity, within the PMIP-2 project using identical glacial boundary conditions, shows the same discrepancy between different models [*Weber et al.*, 2007]. Results of the CLIMBER-2 model are most similar to simulations performed with the CCSM climate model by *Shin et al.* [2003], who also found a shoaling and a weakening of the Atlantic meridional circulation, a pronounced increase of salinity and an intensification of AABW formation. This type of glacial ocean circulation changes is supported by proxy data for Atlantic meridional overturning [*McManus et al.*, 2004; *Lynch-Stieglitz et al.*, 2007], and a dominance of low ^{13}C and ^{14}C Antarctic water in the glacial Atlantic ocean below 2–2.5 km depth [*Duplessy et al.*, 1988; *Curry and Oppo*, 2005; *Robinson et al.*, 2005].

[35] These changes in AABW, and the associated increase in DIC in the deep North Atlantic, explain about 40 ppmv of the glacial CO_2 drawdown. An additional 40 ppmv decrease in atmospheric CO_2 is a consequence of increased nutrient utilization in the in Atlantic and Indian sectors of the sub-Antarctic Ocean, as reconstructed from proxy data [*Kohfeld et al.*, 2005]. Although the total ocean export flux is enhanced by only 24%, the proximity to the AABW formation region increases the sensitivity of atmospheric CO_2 to the biological pump here [*Marinov et al.*, 2006]. Without increased nutrient utilization, we are not able to explain the absence of a glacial to interglacial $\delta^{13}CO_2$ change recorded in the ice cores [*Smith et al.*, 1999].

[36] In total, five mechanisms well supported by proxy data and represented in the G to GNLSC simulations are together able to explain a 65 ppmv drop in CO_2 (Table 3), as compared to 80–90 ppmv recorded in the ice cores. The shortfall could be due to other, less well documented mechanisms, or possibly due a quantitative underestimation of the mechanisms as captured in our model. For example, simulated decrease in global mean annual surface air temperature in this series of experiments is 5°C and thus in the lower part of the best estimate range of 5.8° ± 1.4°C found by *Schneider von Deimling et al.* [2006a] by constraining a large model ensemble with proxy data. A greater

cooling would have enhanced several of the mechanisms considered here. We have not accounted for changes in methane hydrate storages which may partly contribute to glacial-interglacial changes in atmospheric CO_2 and $\delta^{13}CO_2$ [*Maslin and Thomas*, 2003]. A record of diatom resting spore abundance in the Antarctic analyzed recently by *Abelmann et al.* [2006] indicate extensive phytoplankton blooms during the LGM across the entire Atlantic sector of the Antarctic Circumpolar Current. Accounting for complete nutrients utilization in the glacial Antarctic Ocean would definitely enhance CO_2 drawdown in the model, but this it is not supported by the other proxies such as Cd/P ratio [e.g., *Elderfield and Rickaby*, 2000]. Increased export production in the northwest Pacific and equatorial regions of the Atlantic and Indian Oceans during the LGM [*Kohfeld et al.*, 2005] is another mechanism of lowering glacial CO_2 not considered in our study.

[37] CO_2 changes from the different mechanisms probably follow a distinct sequence around the glacial cycle. The CO_2 drawdown based on physical changes in ocean circulation is probably most important in the early stages of glaciation. An ice sheet nucleates in response to insolation changes toward the end of an interglacial climate state, with interglacial CO_2 levels. The ice sheet modifies the climate of the North Atlantic, but would initially have had minor climate impacts elsewhere. Both cooling and retention of freshwater in the ice sheet would make NADW denser. The cooling of North Atlantic would lead to initial CO_2 drawdown, an increase of the Southern Hemisphere sea ice cover, and consequent intensification of AABW which gradually getting dense and starts to replace NADW in the abyssal Atlantic. These circulation changes would result in cooling of the deep ocean and additional lowering of the atmospheric CO_2. Fertilization of the sub-Antarctic Ocean probably kicks in only later during a glacial stage [*Kohfeld et al.*, 2005]. Dust fluxes in Antarctica only increase from interglacial values when the $\delta^{18}O$ is at its negative extreme, in the coldest of the cold climates [*Ridgwell*, 2003; *Wolff et al.*, 2006].

[38] **Acknowledgments.** We thank Andy Ridgwell and an anonymous reviewer for very detailed and constructive comments on the manuscript.

References

Abelmann, A., R. Gersonde, G. Cortese, G. Kuhn, and V. Smetacek (2006), Extensive phytoplankton blooms in the Atlantic sector of the glacial Southern Ocean, *Paleoceanography*, *21*, PA1013, doi:10.1029/2005PA001199.

Adkins, J. F., K. McIntyre, and D. P. Schrag (2002), The salinity, temperature, and $\delta^{18}O$ of the glacial deep ocean, *Science*, *298*, 1769–1773.

Anderson, D. M., and D. Archer (2002), Glacial-interglacial stability of ocean pH inferred from foraminifer dissolution rates, *Nature*, *416*, 70–73.

Archer, D. E. (1991), Modeling the calcite lysocline, *J. Geophys. Res.*, *96*, 17,037–17,050.

Archer, D. (1996), A data-driven model of the global calcite lysocline, *Global Biogeochem. Cycles*, *10*, 511–526.

Archer, D. E., and E. Maier-Reimer (1994), Effect of deep-sea sedimentary calcite preservation on atmospheric CO_2 concentration, *Nature*, *367*, 260–264.

Archer, D., A. Winguth, D. Lea, and N. Mahowald (2000), What caused the glacial/interglacial atmospheric pCO_2 cycles?, *Rev. Geophys.*, *38*, 159–189.

Archer, D. E., J. L. Morford, and S. R. Emerson (2002), A model of suboxic sedimentary diagenesis suitable for automatic tuning and gridded global domains, *Global Biogeochem. Cycles*, *16*(1), 1017, doi:10.1029/2000GB001288.

Archer, D., P. Martin, B. Buffett, V. Brovkin, S. Rahmstorf, and A. Ganopolski (2004), The importance of ocean temperature to global biogeochemistry, *Earth Planet. Sci. Lett.*, *222*, 333–348.

Berger, A. L. (1978), Long-term variations of daily insolation and Quaternary climatic changes, *J. Atmos. Sci.*, *35*, 2362–2368.

Bird, M. I., J. Lloyd, and G. D. Farquhar (1994), Terrestrial carbon storage at the LGM, *Nature*, *371*, 566.

Bopp, L., K. E. Kohfeld, C. Le Quéré, and O. Aumont (2003), Dust impact on marine biota and atmospheric CO_2 during glacial periods, *Paleoceanography*, *18*(2), 1046, doi:10.1029/2002PA000810.

Broecker, W. S., and T. H. Peng (1982), *Tracers in the Sea*, Lamont-Doherty Geol. Obs. of Columbia Univ., Palisades, New York.

Broecker, W. S., and T.-H. Peng (1987), The role of $CaCO_3$ compensation in the glacial to interglacial atmospheric CO_2 change, *Global Biogeochem. Cycles*, *1*, 15–29.

Brovkin, V., J. Bendtsen, M. Claussen, A. Ganopolski, C. Kubatzki, V. Petoukhov, and A. Andreev (2002a), Carbon cycle, vegetation, and climate dynamics in the Holocene: Experiments with the CLIMBER-2 model, *Global Biogeochem. Cycles*, *16*(4), 1139, doi:10.1029/2001GB001662.

Brovkin, V., M. Hofmann, J. Bendtsen, and A. Ganopolski (2002b), Ocean biology could control atmospheric $\delta^{13}C$ during glacial-interglacial cycle, *Geochem. Geophys. Geosyst.*, *3*(5), 1027, doi:10.1029/2001GC000270.

Catubig, N., D. E. Archer, R. Francois, P. deMenocal, and W. Howard (1998), Global deep-sea burial rate of calcium carbonate during the Last Glacial Maximum, *Paleoceanography*, *13*, 298–310.

Crowley, T. J. (1995), Ice-age terrestrial carbon changes revisited, *Global Biogeochem. Cycles*, *9*, 377–389.

Curry, W. B., and D. W. Oppo (2005), Glacial water mass geometry and the distribution of $\delta^{13}C$ of ΣCO_2 in the western Atlantic Ocean, *Paleoceanography*, *20*, PA1017, doi:10.1029/2004PA001021.

Duplessy, J. C., N. J. Shackleton, R. G. Fairbanks, L. Labeyrie, and D. Oppo (1988), Deep water source variations during the last climatic cycle and their impact on the global deep water circulation, *Paleoceanography*, *3*, 343–360.

Elderfield, H., and R. E. M. Rickaby (2000), Oceanic Cd/P ratio and nutrient utilization in the glacial Southern Ocean, *Nature*, *405*, 305–310.

Feely, R. A., C. L. Sabine, K. Lee, W. Berelson, J. Kleypas, V. J. Fabry, and F. J. Millero (2004), Impact of anthropogenic CO_2 on the $CaCO_3$ system in the oceans, *Science*, *305*, 362–366.

Foster, G. L., and D. Vance (2006), Negligible glacial-interglacial variation in continental chemical weathering rates, *Nature*, *444*, 918–921.

Francois, L. M., Y. Godderis, P. Warnant, G. Ramstein, N. de Noblet, and S. Lorenz (1999), Carbon stocks and isotopic budgets of the terrestrial biosphere at mid-Holocene and last glacial maximum times, *Chem. Geol.*, *159*, 163–189.

Ganopolski, A., S. Rahmstorf, V. Petoukhov, and M. Claussen (1998), Simulation of modern and glacial climates with a coupled global model of intermediate complexity, *Nature*, *391*, 351–356.

Ganopolski, A., V. Petoukhov, S. Rahmstorf, V. Brovkin, M. Claussen, A. Eliseev, and C. Kubatzki (2001), CLIMBER-2: A climate system model of intermediate complexity. part II: Model sensitivity, *Clim. Dyn.*, *17*, 735–751.

Gersonde, R., X. Crosta, A. Abelmann, and L. Armand (2005), Sea-surface temperature and sea ice distribution of the Southern Ocean at the EPILOG Last Glacial Maximum—A circum-Antarctic view based on siliceous microfossil records, *Quat. Sci. Rev.*, *24*, 869–896.

Gildor, H., E. Tziperman, and J. R. Toggweiler (2002), Sea ice switch mechanism and glacial-interglacial CO_2 variations, *Global Biogeochem. Cycles*, *16*(3), 1032, doi:10.1029/2001GB001446.

Harrison, S. P., and A. I. Prentice (2003), Climate and CO_2 controls on global vegetation distribution at the Last Glacial Maximum:

Analysis based on palaeovegetation data, biome modelling and palaeoclimate simulations, *Global Change Biol.*, *9*, 983–1004.
Hewitt, C. D., A. J. Broccoli, J. F. B. Mitchell, and R. J. Stouffer (2001), A coupled model study of the Last Glacial Maximum: Was part of the North Atlantic relatively warm?, *Geophys. Res. Lett.*, *28*, 1571–1574.
Iglesias-Rodríguez, M. D., C. W. Brown, S. C. Doney, J. Kleypas, D. Kolber, Z. Kolber, P. K. Hayes, and P. G. Falkowski (2002), Representing key phytoplankton functional groups in ocean carbon cycle models: Coccolithophorids, *Global Biogeochem. Cycles*, *16*(4), 1100, doi:10.1029/2001GB001454.
Jahn, A., M. Claussen, A. Ganopolski, and V. Brovkin (2005), Quantifying the effect of vegetation dynamics on the climate of the Last Glacial Maximum, *Clim. Past*, *1*, 1–7.
Jin, X., N. Gruber, J. P. Dunne, J. L. Sarmiento, and R. A. Armstrong (2006), Diagnosing the contribution of phytoplankton functional groups to the production and export of particulate organic carbon, $CaCO_3$, and opal from global nutrient and alkalinity distributions, *Global Biogeochem. Cycles*, *20*, GB2015, doi:10.1029/2005GB002532.
Joos, F., S. Gerber, I. C. Prentice, B. L. Otto-Bliesner, and P. J. Valdes (2004), Transient simulations of Holocene atmospheric carbon dioxide and terrestrial carbon since the Last Glacial Maximum, *Global Biogeochem. Cycles*, *18*, GB2002, doi:10.1029/2003GB002156.
Keeling, R. F., and B. B. Stephens (2001), Antarctic sea ice and the control of Pleistocene climate instability, *Paleoceanography*, *16*, 112–131.
Kim, S. J., G. M. Flato, and G. J. Boer (2003), A coupled climate model simulation of the Last Glacial Maximum, part 2: Approach to equilibrium, *Clim. Dyn.*, *20*, 635–661.
Kitoh, A., S. Murakami, and H. Koide (2001), A simulation of the Last Glacial Maximum with a coupled atmosphere-ocean GCM, *Geophys. Res. Lett.*, *28*, 2221–2224.
Kleypas, J. A. (1997), Modeled estimates of global reef habitat and carbonate production since the Last Glacial Maximum, *Paleoceanography*, *12*, 533–545.
Kohfeld, K. E., C. Le Quere, S. P. Harrison, and R. F. Anderson (2005), Role of marine biology in glacial-interglacial CO_2 cycles, *Science*, *308*, 74–78.
Köhler, P., H. Fischer, G. Munhoven, and R. E. Zeebe (2005), Quantitative interpretation of atmospheric carbon records over the last glacial termination, *Global Biogeochem. Cycles*, *19*, GB4020, doi:10.1029/2004GB002345.
Lambeck, K., and J. Chappell (2001), Sea level change through the last glacial cycle, *Science*, *292*, 679–686.
Lynch-Stieglitz, J., et al. (2007), Atlantic meridional overturning circulation during the Last Glacial Maximum, *Science*, *316*, 66–69.
Mahowald, N., K. Kohfeld, M. Hansson, Y. Balkanski, S. P. Harrison, I. C. Prentice, M. Schulz, and H. Rodhe (1999), Dust sources and deposition during the last glacial maximum and current climate: A comparison of model results with paleodata from ice cores and marine sediments, *J. Geophys. Res.*, *104*, 15,895–15,916.
Maier-Reimer, E., and R. Bacastow (1990), Modelling of geochemical tracers in the ocean, in *Climate-Ocean Interaction*, edited by M. E. Schlesinger, pp. 233–267, Kluwer Acad., Norwell, Mass.
Marinov, I., A. Gnanadesikan, J. R. Toggweiler, and J. L. Sarmiento (2006), The Southern Ocean biogeochemical divide, *Nature*, *441*, 964–967.
Martin, J. H., G. A. Knauer, D. M. Karl, and W. W. Broenkow (1987), VERTEX: Carbon cycling in the northeast Pacific, *Deep Sea Res., Part A*, *34*, 267–285.
Martin, P., D. Archer, and D. Lea (2002), The role of deep sea temperature change in the glacial carbon cycle, *Geochim. Cosmochim. Acta*, *66*, A488–A488.
Martin, P., D. Archer, and D. W. Lea (2005), Role of deep sea temperature in the carbon cycle during the last glacial, *Paleoceanography*, *20*, PA2015, doi:10.1029/2003PA000914.
Maslin, M. A., and E. Thomas (2003), Balancing the deglacial global carbon budget: The hydrate factor, *Quat. Sci. Rev.*, *22*, 1729–1736.
Matsumoto, K., J. L. Sarmiento, and M. A. Brzezinski (2002), Silicic acid leakage from the Southern Ocean: A possible explanation for glacial atmospheric pCO_2, *Global Biogeochem. Cycles*, *16*(3), 1031, doi:10.1029/2001GB001442.
McManus, J. F., R. Francois, J. M. Gherardi, L. D. Keigwin, and S. Brown-Leger (2004), Collapse and rapid resumption of Atlantic meridional circulation linked to deglacial climate changes, *Nature*, *428*, 834–837.
Milliman, J. D. (1993), Production and accumulation of calcium carbonate in the ocean: Budget of a nonsteady state, *Global Biogeochem. Cycles*, *7*, 927–957.
Milliman, J. D., and A. W. Droxler (1996), Neritic and pelagic carbonate sedimentation in the marine environment: Ignorance is not bliss, *Geol. Rundsch.*, *85*, 496–504.
Munhoven, G. (2002), Glacial-interglacial changes of continental weathering: Estimates of the related CO_2 and HCO_3–Flux variations and their uncertainties, *Global Planet. Change*, *33*, 155–176.
Otto, D., D. Rasse, J. Kaplan, P. Warnant, and L. Francois (2002), Biospheric carbon stocks reconstructed at the Last Glacial Maximum: Comparison between general circulation models using prescribed and computed sea surface temperatures, *Global Planet. Change*, *33*, 117–138.
Paillard, D., and F. Parrenin (2004), The Antarctic ice sheet and the triggering of deglaciations, *Earth Planet. Sci. Lett.*, *227*, 263–271.
Peacock, S., E. Lane, and J. M. Restrepo (2006), A possible sequence of events for the generalized glacial-interglacial cycle, *Global Biogeochem. Cycles*, *20*, GB2010, doi:10.1029/2005GB002448.
Peltier, W. R. (1994), Ice age paleotopography, *Science*, *265*, 195–201.
Petit, J. R., et al. (1999), Climate and atmospheric history of the past 420,000 years from the Vostok ice core, Antarctica, *Nature*, *399*, 429–436.
Petoukhov, V., A. Ganopolski, V. Brovkin, M. Claussen, A. Eliseev, C. Kubatzki, and S. Rahmstorf (2000), CLIMBER-2: A climate system model of intermediate complexity. part I: Model description and performance for present climate, *Clim. Dyn.*, *16*, 1–17.
Prentice, I. C., and D. Jolly (2000), Mid-Holocene and glacial-maximum vegetation geography of the northern continents and Africa, *J. Biogeogr.*, *27*, 507–519.
Rayner, N. A., D. E. Parker, E. B. Horton, C. K. Folland, L. V. Alexander, D. P. Rowell, E. C. Kent, and A. Kaplan (2003), Global analyses of sea surface temperature, sea ice, and night marine air temperature since the late nineteenth century, *J. Geophys. Res.*, *108*(D14), 4407, doi:10.1029/2002JD002670.
Rea, D. K. (1994), The paleoclimatic record provided by eolian deposition in the deep sea: The geologic history of wind, *Rev. Geophys.*, *32*, 159–196.
Ridgwell, A. J. (2003), Implications of the glacial CO_2 "iron hypothesis" for Quaternary climate change, *Geochem. Geophys. Geosyst.*, *4*(9), 1076, doi:10.1029/2003GC000563.
Ridgwell, A., and J. C. Hargreaves (2007), Regulation of atmospheric CO_2 by deep-sea sediments in an Earth system model, *Global Biogeochem. Cycles*, *21*, GB2008, doi:10.1029/2006GB002764.
Ridgwell, A., and R. E. Zeebe (2005), The role of the global carbonate cycle in the regulation and evolution of the Earth system, *Earth Planet. Sci. Lett.*, *234*, 299–315.
Robinson, L. F., J. F. Adkins, L. D. Keigwin, J. Southon, D. P. Fernandez, S. L. Wang, and D. S. Scheirer (2005), Radiocarbon variability in the western North Atlantic during the last deglaciation, *Science*, *310*, 1469–1473.
Ruddiman, W. F. (2001), *Earth's Climate: Past and Future*, 465 pp., W. H. Freeman, New York.
Scheffer, M., V. Brovkin, and P. M. Cox (2006), Positive feedback between global warming and atmospheric CO_2 concentration inferred from past climate change, *Geophys. Res. Lett.*, *33*, L10702, doi:10.1029/2005GL025044.
Schmittner, A. (2003), Southern Ocean sea ice and radiocarbon ages of glacial bottom waters, *Earth Planet. Sci. Lett.*, *213*, 53–62.
Schneider von Deimling, T., A. Ganopolski, H. Held, and S. Rahmstorf (2006a), How cold was the Last Glacial Maximum?, *Geophys. Res. Lett.*, *33*, L14709, doi:10.1029/2006GL026484.
Schneider von Deimling, T., H. Held, A. Ganopolski, and S. Rahmstorf (2006b), Climate sensitivity estimated from ensemble simulations of glacial climate, *Clim. Dyn.*, *27*, 149–163.
Shackleton, N. J. (1977), Carbon 13 in Uvigerina: Tropical rainforest history and the equatorial Pacific carbonate dissolution cycles, in *The Fate of Fossil Fuel CO_2 in the Oceans*, edited by N. R. Andersen and A. Malahoff, pp. 401–428, Plenum, New York.
Shin, S. I., Z. Liu, B. Otto-Bliesner, E. C. Brady, J. E. Kutzbach, and S. P. Harrison (2003), A simulation of the last glacial maximum climate using the NCAR-CCSM, *Clim. Dyn.*, *20*, 127–151.
Siegenthaler, U., et al. (2005), Stable carbon cycle-climate relationship during the late Pleistocene, *Science*, *310*, 1313–1317.
Sigman, D. M., and E. A. Boyle (2000), Glacial/interglacial variations in atmospheric carbon dioxide, *Nature*, *407*, 859–869.
Smith, H. J., H. Fischer, M. Wahlen, D. Mastroianni, and B. Deck (1999), Dual modes of the carbon cycle since the Last Glacial Maximum, *Nature*, *400*, 248–250.
Stephens, B. B., and R. F. Keeling (2000), The influence of Antarctic sea ice on glacial-interglacial CO_2 variations, *Nature*, *404*, 171–174.
Stocker, T. F., D. G. Wright, and L. A. Mysak (1992), A zonally averaged, coupled ocean atmosphere model for paleoclimate studies, *J. Clim.*, *5*, 773–797.
Toggweiler, J. R., J. L. Russell, and S. R. Carson (2006), Midlatitude westerlies, atmospheric CO_2, and climate change during the ice ages,

Paleoceanography, *21*, PA2005, doi:10.1029/2005PA001154.
Torn, M. S., and J. Harte (2006), Missing feedbacks, asymmetric uncertainties, and the underestimation of future warming, *Geophys. Res. Lett.*, *33*, L10703, doi:10.1029/2005GL025540.
Waelbroeck, C., L. Labeyrie, E. Michel, J. C. Duplessy, J. F. McManus, K. Lambeck, E. Balbon, and M. Labracherie (2002), Sea-level and deep water temperature changes derived from benthic foraminifera isotopic records, *Quat. Sci. Rev.*, *21*, 295–305.
Watson, A. J., and A. C. N. Garabato (2006), The role of Southern Ocean mixing and upwelling in glacial-interglacial atmospheric CO_2 change, *Tellus, Ser. B*, *58*, 73–87.
Weber, S. L., S. S. Drijfhout, A. Abe-Ouchi, M. Crucifix, M. Eby, A. Ganopolski, S. Murakami, B. Otto-Bliesner, and W. R. Peltier (2007), The modern and glacial overturning circulation in the Atlantic ocean in PMIP coupled model simulations, *Clim. Past*, *3, 51–64.*
Wolff, E. W., et al. (2006), Southern Ocean sea-ice extent, productivity and iron flux over the past eight glacial cycles, *Nature*, *440*, 491–496.

D. Archer, Department of Geophysical Sciences, University of Chicago, 5734 South Ellis Avenue, Chicago, IL 60637, USA.
V. Brovkin, A. Ganopolski, and S. Rahmstorf, Potsdam Institute for Climate Impact Research, P.O. Box 601203, Potsdam, Germany. (victor@pik-potsdam.de)